JOURNAL OF PROPULSION AND POWER
Vol. 20, No. 4, July–August 2004

Instability Mechanisms in a Premixed Prevaporized Combustor

D. Bernier,* F. Lacas,† and S. Candel‡
Ecole Centrale Paris and Centre National de la Recherche Scientifique, 92295 Châtenay-Malabry, France

Instabilities in a premixed prevaporized 150-kW model scale combustor are investigated experimentally. The injector fed with liquid heptane and preheated air features two sets of swirling blades that induce flow rotation in the same direction (corotative) or in the opposite direction (counter-rotative). The flame is stabilized with swirl behind a dump. Instabilities occur in the low-frequency range around 400 Hz corresponding to a quarter-wave mode acoustic coupling of the system. Simultaneous measurements of pressure and heat-release oscillations and phase-locked CH chemiluminescence images are used to characterize the combustion dynamics. In both corotative (COS) and counter-rotative (CNS) cases, the reaction region moves closer to the injector when the flame becomes unstable by about one-third of the stabilization distance under normal operation. Experiments indicate that the two swirl configurations have distinct domains of instability. The instability boundary separating stable and unstable regions can be defined in terms of a critical velocity v_c, which depends on the equivalence ratio Φ, air injection temperature T_{inj}, and swirl geometry. In the coswirl configuration, instabilities occur when the injection velocity is lower than the critical velocity [$u < v_c(\Phi, T_{\text{inj}}; \text{COS})$], while they appear for velocities higher than the critical velocity in the counterswirl geometry [$u > v_c(\Phi, T_{\text{inj}}; \text{CNS})$]. In a range of conditions corresponding to low injection velocities, reduced eqivalence ratio, and for the coswirl configuration, an unsteady flashback takes place in which the flame moves periodically in and out of the fuel premixer. This mechanism is related to the existence of a low-velocity region near the injector exit plane. Observations of the space–time development of the heat release under unstable operation indicate that the oscillations are significantly influenced by the swirl geometry and are caused by different mechanisms. The coswirl configuration features a central recirculation, which gives rise to periodic vortex roll-up, convection, and sudden release of heat when the vortices impinge on the lateral walls. In the counterswirl geometry there are no identifiable flow structure, but the heat-release pattern is convected periodically in the chamber. Estimates of the delay times associated with the two mechanisms support the view that coswirl instabilities are driven by vortex roll-up, whereas counterswirl instabilities are probably sustained by equivalence-ratio inhomogeneities.

I. Introduction

THE increasing need for power and the developing air and ground transportation induce a continuous growth in pollutant emissions. This has an important impact on the environment and on human health. To reduce pollution, regulations have become progressively more stringent. New ideas and methods are actively explored to diminish emission levels. In the domain of gas turbines and aircraft jet engines, it has been shown that the lean premixed combustion technology allows considerable reductions of NOx levels in the exhaust streams.[1,2] In devices where fuel is in liquid form, it is injected as a spray that is first prevaporized to form a lean mixture. Unfortunately, systems using this lean premixed prevaporized mode of operation (LPP) are succeptible to instability and feature oscillations that can reach unacceptable levels. These instabilities enhance heat loads on the combustor walls and induce mechanical vibrations reducing the performance and life duration of the system. Instabilities sometimes lead to a flashback process in which the flame moves periodically into the fuel premixer. Excessive oscillation can also lead to flame blow-off. In most cases, the instability phenomenon appears as a coupled oscillation of heat release and pressure inside the combustion chamber.[3,4]

In the standard mode of LPP combustor operation, a fuel is injected in the form of spray. If the spray is not rapidly vaporized, it yields equivalence-ratio gradients that create high-temperature regions increasing the NOx emission level. The injector is therefore designed to prevaporize fuel and premix it with air in order to get uniform temperature and mixture ratio profiles before combustion. To be effective, an injector has to be as short as possible. On one hand, if the time delay between injection and combustion is too long the vaporized mixture can autoignite inside the injector element leading to a rapid degradation of this device. On the other hand, this element has to be long enough to enable droplets vaporization. This optimization tradeoff is described for example by Cowell and Smith.[5]

Combustion instabilities mechanisms involve coupled processes of fluid flow, vaporization, heat release, and acoustic feedback. These interactions are quite sensitive to the different operating parameters (geometry, fuel and air injection, boundary conditions), as shown in the many studies carried out over the past 50 years. Although the experimental base is quite extensive, there is a lack of predictive tools for combustion instabilities (see the reviews of Candel[6] and Schadow and Gutmark[7] and the recent book edited by Yang and Anderson.[8]) One central question is to identify the mechanism and conditions that lead to the coupling between combustion and acoustic modes driving the system into in stability. The general objective is to devise suitable models of the combustion dynamics allowing developments of predictive methods and control concepts.

A considerable amount of work deals with the mechanisms of combustion instabilities in low-NOx premixed burners. The effect of incomplete fuel–air mixing on flame stability and pollutant emission in a premixed combustor is examined by Shih et al.[9] Poinsot et al.[10] and Schadow and Gutmark[7] study the links between vortex shedding and instabilities. The influence of swirl on combustion stability is considered in various respects. Sivasegaram and Whitelaw[11] study the oscillations of premixed flames behind different types of obstacles as a function of swirl. Stephens et al.[12] analyze the effect of swirl on droplet distribution in the spray and on the velocity profiles. Cha et al.[13] examine the stabilization distance of a lifted

Received 24 July 2000; revision received 18 October 2002; accepted for publication 3 January 2004.

*Ph.D. Student; currently Engineer, Snecma Moteurs, 77550 Villaroche, France.
†Research Scientist, Laboratoire EM2C, CNRS, Ecole Centrale Paris.
‡Professor, Ecole Centrale Paris and Institut Universitaire de France. Associate Member AIAA.

nonpremixed flame as a function of swirl. Yegian and Cheng[14] determine a link between a threshold in the swirl number and flashback. The mechanism of flashback is first reviewed by Plee and Mellor[15] in an early paper. Guin[16] gives a more recent classification of autoignition and flashback for different kinds of premixed injection systems. On the theoretical side, some recent studies indicate that instabilities in lean premixed systems can be driven by periodic perturbations in the equivalence ratio[17] or by fluctuations of the oncoming flow velocity at the flame holder.[18]

Although many publications deal with lean premixed combustors fed by gaseous fuels (methance or natural gas), less data are available for the case of liquid-fueled low-NOx combustors. There are however important practical applications of such devices in particular in jet engines and gas turbines.

The present study is concerned with the latter situation. Experiments on self-sustained oscillations are carried out on a laboratory-scale premixed prevaporized combustor described in Sec. II. This test rig uses heptance (C_7H_{16}) as liquid fuel and features an injector with swirl. The various types of instabilities of this system are examined in Sec. III for two swirl configurations (coswirl and counterswirl). Mechanisms leading to combustion oscillations are discussed in Sec. IV. The phenomenon of flashback during stable and unstable operating conditions is also observed and discussed in the last section.

II. Experimental Setup

A. Injector and Combustor

The laboratory-scale premixed prevaporized combustor used in these experiments was designed to study combustion dynamics and control of instabilities. The premixing injector is sketched in Fig. 1. The main part of this injector features the two swirlers, which can be set in two positions with either co- or counter-rotative blades. These two configurations induce two types of swirling flows that decisively influence the flame structure and stability as discussed later in this paper. Circumferential holes allow air cooling of the walls and cup holes prevent a direct flame attachment on the injector exit.

The level of rotation induced by the injector can be characterized by a swirl number defined by the ratio of tangential and axial momentum fluxes[19]

$$S = \frac{\int_0^R 2\pi\rho u_z u_\theta r^2\,\mathrm{d}r}{R\int_0^R 2\pi\rho u_z^2 r\,\mathrm{d}r} \tag{1}$$

where u_z and u_θ are respectively axial and tangential velocities and R is the flow radius. In the two swirl configurations, swirl number was experimentally determined from velocity profiles measurements carried out in cold-flow experiments.[20] The estimated swirl number is $S = 0.22$ in the coswirl configuration and $S = 0.07$ in the counterswirl geometry. In both cases the swirl number is relatively low. According to a classification proposed by Claypole and Syred,[21] strong swirl prevails for $S > 0.6$. The flow is weakly swirled below that value.

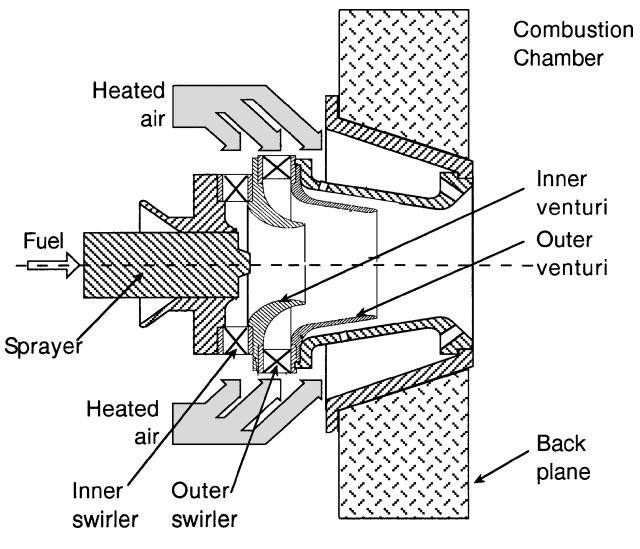

Fig. 1 Sketch of the LPP injector.

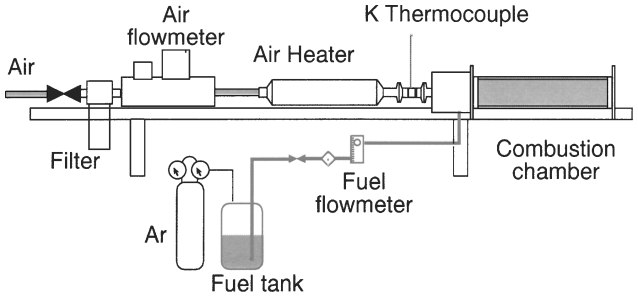

Fig. 2 General layout of the experimental setup.

An overview of the setup is shown in Fig. 2. The burner is supplied with electrically preheated air with a temperature reaching 600 K. Air maximum flow rate is 100 g s^{-1}. The preheated air passes through the premixing injector before entering the combustion chamber. Heptane is used as liquid fuel with a maximum flow rate of 4 g s^{-1}. The overall equivalence ratio of the mixture is defined by $\Phi = (\dot{m}_f/\dot{m}_a)/(\dot{m}_f/\dot{m}_a)_s$, where $\dot{m}_f$ and $\dot{m}_a$ are respectively the fuel and air mass flow rates and s designates stoichiometric conditions. This ratio lies between 0.4 and 1.0. The heat release in this combustor can reach 170 kW (for the maximum fuel flow rate of 4 g s^{-1}). The combustion chamber is 52 cm long with a square section of 10×10 cm^2. Its side walls are made of fused silica allowing full optical access to the flame. A set of plugs located on the upper wall of the combustor is used for unsteady pressure measurements.

B. Diagnostics

Pressure oscillations in the combustion chamber are detected with a $\frac{1}{4}$-in. (6.3 mm) microphone (Brüel & Kjaer, type 4136) mounted on a waveguide and equipped with a type 2669 preamplifier and a signal conditioning amplifier (Nexus 2690-AOS2). To avoid spectral aliasing, the analog signal is filtered before sampling. The bandpass extends from 0.1 Hz to 3 kHz. Above 3 kHz, the amplitude falls by 40 dB/decade. The cutoff frequency is high enough not to perturb the signal in the useful range below 1 kHz. The waveguide entrance orifice is located at 5.5 cm from the injector. The microphone is positioned at 67 cm from the chamber wall. The duct is water cooled, and a small flow of fresh air prevents burned gases from damaging the microphone and cools the tube down. The tube is terminated by an infinite coil, which eliminates reflected waves. Given that fresh air ciculates inside the tubing, the amplitude is approximately constant in the 67-cm waveguide, but one has to account for the time delay of 2 ms, which corresponds to the propagation of sound at ambient temperature ($c = 340$ ms^{-1}) from the tube entrance to the sensor.

The heat-release oscillations are measured with a photomultiplier tube (Electron Tubes, Inc., Type 9129 SB). The emission originating from the flame is focussed on the tube diaphragm by a converging lense (focal length = 64 cm) and passes through an interferential filter ($\Delta\lambda = 410$–460 nm) centered on the CH* radical $B^2\Sigma \rightarrow X^2\Pi$ transition at 431.5 nm, which constitutes a good tracer of the reaction zone.[22,23] The lens faces the flame front near the injector. Its diameter is sufficient to focus the light emitted from most of the flame for the different combustion regimes.

The photomultiplier tube and microphone signals are processed to extract the spectral content of the oscillations. This is done for both diagnostics with a digital oscilloscope (LeCroy, type 9410). The spectral analysis of the signal is obtained with a resolution of 5 Hz and a Nyquist frequency of 2 kHz through a Hamming window. Blocks of 500 points are taken from each fast Fourier transform and averaged over 20 sweeps. The spectral densities are given on a log scale (in decibels).

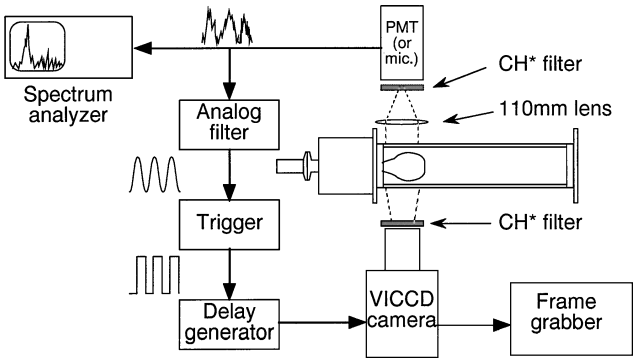

Fig. 3 Sketch of the setup for phase-locked imaging.

A video-intensified charge-coupled device (VICCD) camera (Princeton Instruments, Inc.) is used for flame visualization. The gain and aperture time of the intensifier can be tuned to optimize the resolution using the camera control box and a pulse generator (Princeton Instruments, Inc., type PG200). The lens mounted on the camera is a Nikon 105 mm and 2.8 aperture zoom. An interferential filter is set in front of the lens. The filter bandpass of 410–460 nm is also centered on the 431.5-nm wavelength (corresponding to the $B^2\Sigma \rightarrow X^2\Pi$ transition of CH^* radicals). The magnification is chosen so that the first half of the chamber (24 cm long) can be imaged with a good spatial resolution. Images delivered by the camera are digitized on a PC using a National Instrument data-acquisition board (type PCI-Imaq-1408). The available images all have the same dimensions: 24 cm long, 10 cm high.

The instability is visualized at different instants in the cycle with phase-locked imaging. Figure 3 shows a sketch of the corresponding setup. The video camera is triggered either by the photomultiplier tube or by the microphone signal. To get a suitable trigger, the signal is filtered through an analog low-pass filter (Frequency Devices, Inc., Type 901F) with a cutoff frequency sufficiently greater than the instability frequency. The filtered signal is transformed into a TTL signal by an oscilloscope (Tektronix, type TDS620). The TTL signal is then transmitted to the pulse generator of the VICCD camera. The PG200 delivers a time delay, which is converted into a phase in the instability cycle. The exposure time is also set by the PG200 pulse generator. Best images (lowest noise) are obtained with 5–50 μs exposure times for an averaging of 100 exposures per picture. A time delay of 50 μs corresponds to 2% of the full period at a frequency of 400 Hz.

C. Determination of the Acoustic Eigenmodes of the Burner

Because combustion instabilities are coupled by an acoustic field that is generally close to the eigenmodes of the system, it is worth determining the corresponding eigenfrequencies and mode shapes. We will specifically consider the quarter-wave mode that arises in the experiments. In the range of frequencies of interest ($\leq$1 kHz), acoustic propagation essentially involves plane waves. The acoustic response is then well analyzed with a transfer matrix one-dimensional acoustic model developed earlier[10] and improved in Ref. 24. The upstream boundary condition is obtained from detailed experimental measurements. Lateral walls are assumed adiabatic. The exit is considered to be open to ambient pressure. The model extends from the air heater to the combustor exhaust section. The temperature field is estimated from previous measurements: 520 K in the upstream region, 1500 K inside the combustion chamber. The acoustic impedance of the upstream line has to be determined. The reflection coefficient and corresponding impedance was measured experimentally using the method described in Ref. 25. Basically, this method treats the signals recorded by a set of microphones (here three microphones are used) to separate the pressure field in the duct into upstream and downstream traveling waves. The ratio of these two components provides the reflection coefficient of the device at the end of the tubing. The method was validated in the standard case of a purely rigid wall. Measurements of the reflection coefficient

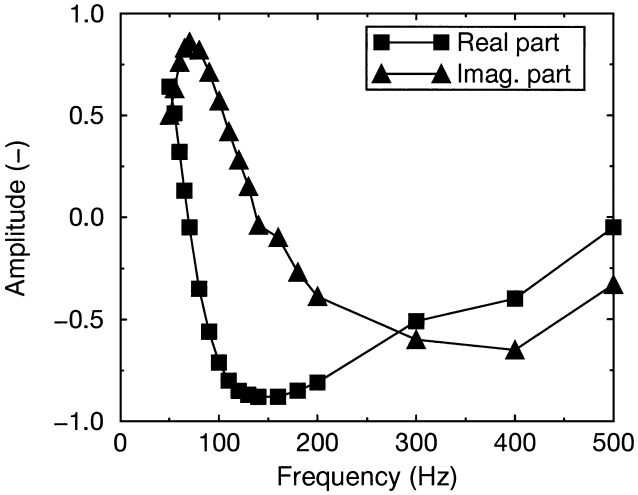

Fig. 4 Reflection coefficient of the air heater upstream line vs frequency.

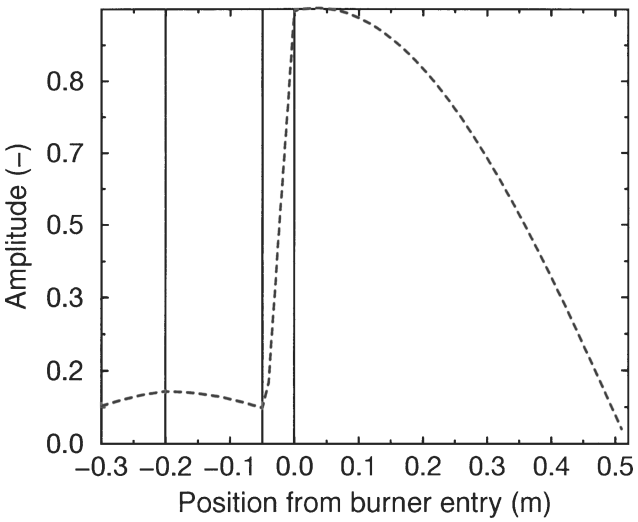

Fig. 5 Structure of the pressure response of the test rig. A volume source located 10 cm from the dump section excites the device at a frequency of 400 Hz.

are given in Fig. 4. The corresponding acoustic impedance features a real part with positive values corresponding to a wave damping. Using these data, one obtains the acoustical response of the burner submitted to a source located in the vicinity of the combustor dump section. The response reaches the largest amplitude near 390 Hz. The structure of this response is given in Fig. 5. This structure indicates that the mode inside the combustion chamber is essentially a quarter-wave oscillation with a pressure node at the burner exit and an antinode at its inlet. We will see below that the oscillations feature frequencies that are close to the eigenfrequency determined in this section. The frequency of the instability does depend to a certain extent on the injector configuration. Also the frequency is not quite identical to that of the quarter-wave mode calculated on a purely acoustic basis.

III. Experimental Results

A. Operating Domains

A wide range of stable and unstable regimes was studied in the coswirling (COS) and counterswirling (CNS) configurations. The regions of stable and unstable operation were mapped out by systematically changing the air and fuel mass flow rates for the two swirl arrangements and for different injection temperatures (Figs. 6 and 7). The burner behavior is controlled by the swirl configuration. Flame stabilization is achieved down to an equivalence ratio

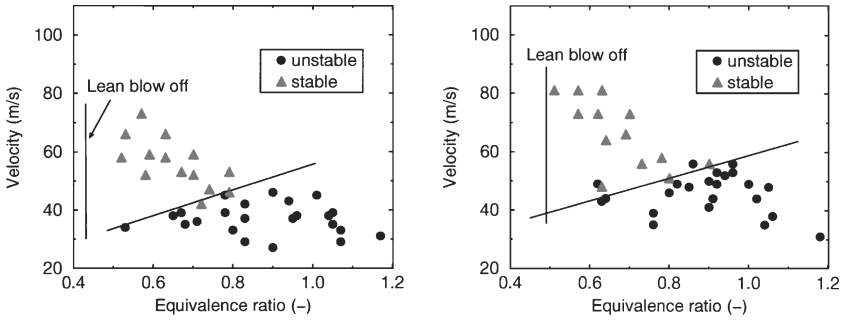

Fig. 6 Operating domain in coswirl configuration (COS): a) T_{inj} = 420–470 K and b) T_{inj} = 520–570 K. Instabilities occur at low injection velocities. The transition between stable and unstable domain is shifted to higher velocities as the temperature is increased.

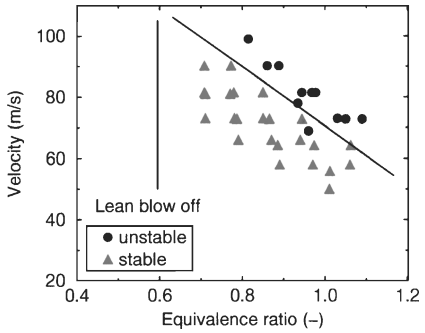

Fig. 7 Operating domain in counter-swirl configuration (CNS): T_{inj} = 520–570 K. For a given equivalence ratio instabilities occur when the velocity exceeds a critical value. This critical value increases with injection temperature.

of 0.4 and for injection velocities from 30 to 80 ms^{-1} in the COS geometry while the lean blow-off limit lies around $\Phi = 0.6$ and velocities between 40 and 100 ms^{-1} in the CNS case. The boundary between stable and unstable regimes can be defined in terms of a critical injection velocity. This velocity is a function of equivalence ratio, injection temperature, and swirl geometry : $v_c = v_c(\Phi, T_{inj}; \text{geom})$.

1) For COS injection, instability is observed in the low velocity range for $u < v_c$, and the critical velocity increases with Φ and T_{inj} ($\Delta v_c/\Delta\Phi > 0$ and $\Delta v_c/\Delta T_{inj} > 0$).

2) For CNS injection, instability occurs when the injection velocity exceeds the critical velocity $v_c < u$ and the critical velocity decreases with Φ but increases with T_{inj} ($\Delta v_c/\Delta\Phi < 0$ and $\Delta v_c/\Delta T_{inj} > 0$).

In both cases one finds by looking at the stability maps from the side and keeping a constant velocity that instability occurs when the equivalence ratio is increased beyond a critical value.

The maps displayed in Fig. 6 and 7 also indicate that instabilities in the COS configuration appear over a wider range of equivalence ratios than in the CNS case (from $\Phi = 0.5$ to 1 vs $\Phi = 0.8$ to 1). They are otherwise less powerful. The maximum pressure level is 140 dB for COS while it exceeds 155 dB in CNS ($p_{ref} = 210^{-5}$ Pa). This is caused in part by the different mean rates of heat release, which for CNS instabilities are more than twice as high as those corresponding to COS instability regimes.

The present instability data differ from those reported in previous studies. For example, experiments carried out by Venkataraman et al.[26] on a lean premixed dump combustor with coaxial injection of gaseous fuel and air with swirl indicate that unstable combustion occurs near lean blowout and not at higher equivalence ratios. This differs from what is observed in the present experiments where instabilities occur over a broad range of equivalence ratios in the working domain of the burner. Also, the distinct behavior of COS and CNS geometries with a marked change in position of the instability domain has not been observed by others.

B. Typical Signals and Spectra

Typical signals and spectral densities of pressure and heat-release oscillations are shown in Fig. 8. The data for both COS and CNS configurations are similar. The instability frequencies are easily identified in the spectral densities of both pressure and heat-release signals. The pressure oscillation amplitudes can be read directly. In COS, the pressure oscillation level is about 130 Pa corresponding to 140 dB, whereas in CNS the oscillation amplitude is about 2500 Pa corresponding to 155 dB ($p_{ref} = 210^{-5}$ Pa).

The coupling between pressure and heat-release oscillations is made evident in Fig. 9 during an intermittent regime, which flips between stable and unstable combustion. One clearly sees in this figure that the signals are correlated during unstable combustion and uncorrelated under stable operation. This is consistent with the Rayleigh criterion,[3] which indicates that pressure and heat-release oscillations should be in phase during an instability. A similar intermittent phenomenon is described by Richards and Janus,[27] but their hysteresis cycles occured on a longer time scale of about 10 s while the flipping time is in the present case of 0.5 s. This timescale between stable and unstable modes is also sensitive to the operating conditions: a slight variation of less than 1% of the air flux can change this timescale by a factor of 10.

C. Imaging

In every observed unstable regime, the instability shifts the mean flame closer to the injector exit by about one-third of the stabilization distance as shown in the time average images of Fig. 10. This has been noticed in previous studies and is responsible in part for the augmentation of heat flux to the injector head. In COS configuration and under stable operation, the highest heat-release point lies at a distance of 3 d_{inj}, whereas during unstable combustion the average position of the reaction zone is at 2 d_{inj} from the back plane. Figure 10 also shows that transition between stable and unstable regimes also differs markedly in the COS and CNS configurations. In COS, transition between stability and instability is quite sharp (within 4% of equivalence-ratio variation), whereas in CNS it is less sensitive to airflow rate variation and appears more progressively as the equivalence ratio is increased.

Instability regimes were observed by phase-locked imaging to visualize the evolution of the reaction zone through the instability cycle. These regimes are defined in Table 1. The corresponding images are displayed in Figs. 11–13. The injector geometry is shown schematically at its actual position in the figures. Three different types of motion are observed.

In the CNS configuration, the instabilities occur at frequencies around 350 Hz and amplitudes of 155 dB. As shown in Fig. 11, the reaction zone is periodically convected downstream, and the total heat release is oscillating between almost zero to full scale. During a short period in the cycle, the flame nearly vanishes.

Table 1 Operating conditions of the presented regimes

Regime	Swirl	Power, kW	Φ	T_{inj}, K	f, Hz	l, m	τ_{inj}, ms	τ_{conv}, ms	τ_c, ms	$\tau_e f$	Amplitude, dB
A	COS	60	0.88	523	435	0.07	0	2.7	0.14	1.2	133
B	COS	77	0.68	523	Stable	——	——	——	——	——	105
C	COS	76	0.91	423	Transition	——	——	——	——	——	110/130
D	COS	60	0.69	523	Stable	——	——	——	——	——	105
E	COS	60	0.73	523	430	——	——	——	——	——	138
F	CNS	110	0.67	573	Stable	——	——	——	——	——	105
G	CNS	110	0.71	573	Stable	——	——	——	——	——	105
H	CNS	110	0.81	573	340	0.12	0.56	2.6	0.17	0.94	153
I	CNS	110	0.97	573	350	——	——	——	——	——	155
J	CNS	102	0.90	573	350	0.11	0.68	2.9	0.14	1.1	155
K	COS	69	0.94	573	430	0.07	0	2.2	0.13	1.0	140
L[a]	COS	33	0.52	523	450	0.043	0	1.8	0.52	1.0	137

[a]L is a flashback regime.

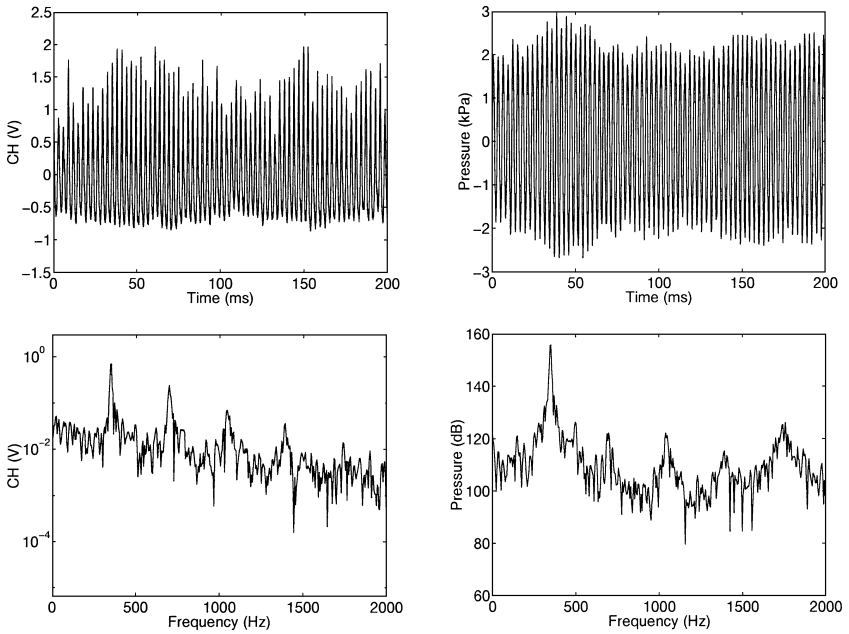

Fig. 8 Typical instability signals and spectral densities. Test conditions: regime I. Inlet temperature T = 573 K, heptane flow rate $\dot{m}_f$ = 2.3 g/s, and Φ = 0.97, CNS. The oscillation is at 350 Hz.

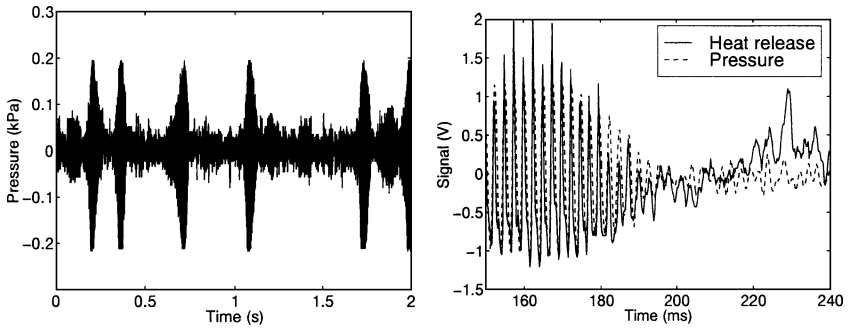

Fig. 9 Flipping between stable and unstable combustion: regime C. Simultaneous evolution of pressure and heat release. The signals are in phase during the instability and uncorrelated during stable operation. Test conditions: inlet temperature T = 423 K, heptane flow rate $\dot{m}_f$ = 1.60 g/s, and Φ = 0.91, COS.

In the COS configuration, the instabilities occur at higher frequencies around 430 Hz and an amplitude of 140 dB. As indicated in Fig. 12, the reaction zone is more compact, and downstream convection is less apparent. The oscillation amplitude is lower than in CNS case. In the COS configuration, cyclic instabilities are generated and develop near the flow axis. The heat-release distribution observed in Fig. 12 is reminiscent of similar patterns, which were noticed in Ref. 10 and were clearly associated with a process of vortex formation and subsequent breakdown. One can infer that the oscillation is driven by a periodic shedding of vortices from the injector wake, which in the COS configuration features a central recirculation zone. The recirculation region interacts with the acoustic field generating vortex patterns. Vortex growth and subsequent breakdown create large fluctuations in heat-release rate, coupling back with the pressure and acoustic field. Vortex structures identified in Fig. 12 (155 and 194 deg) break down during the second part of the cycle.

For a limited range of velocities and equivalence ratios ($u \simeq 30$ m s^{-1}, $\Phi \simeq 0.55$), the flame moves periodically upstream

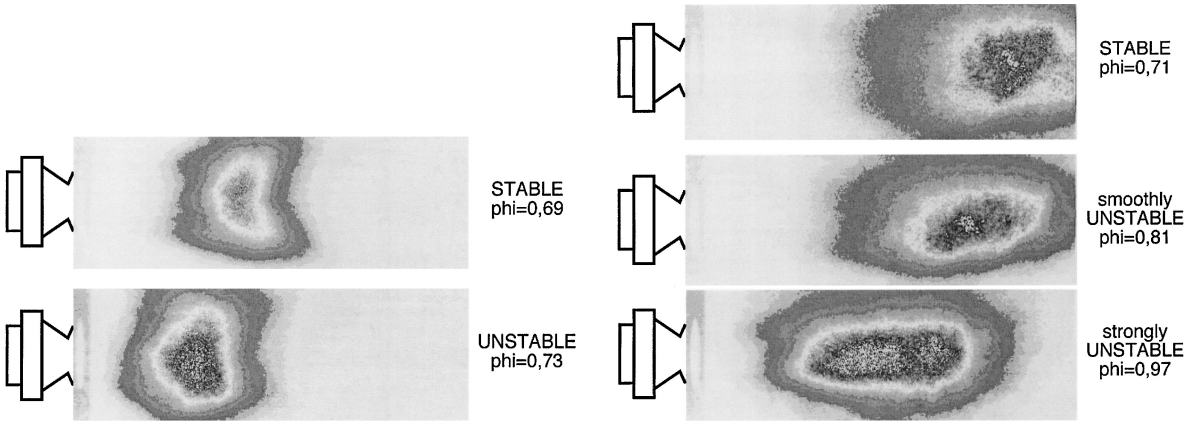

Fig. 10 Transition to instability and its effect on the flame. The flame moves closer to the injector during unstable combustion: a) regime D and E. COS, P = 60 kW, T_{inj} = 523 K; b) regime G, H, I, CNS, P = 110 kW, T_{inj} = 573 K. Transition between stable and unstable regimes is sharper in coswirl than in counterswirl configuration.

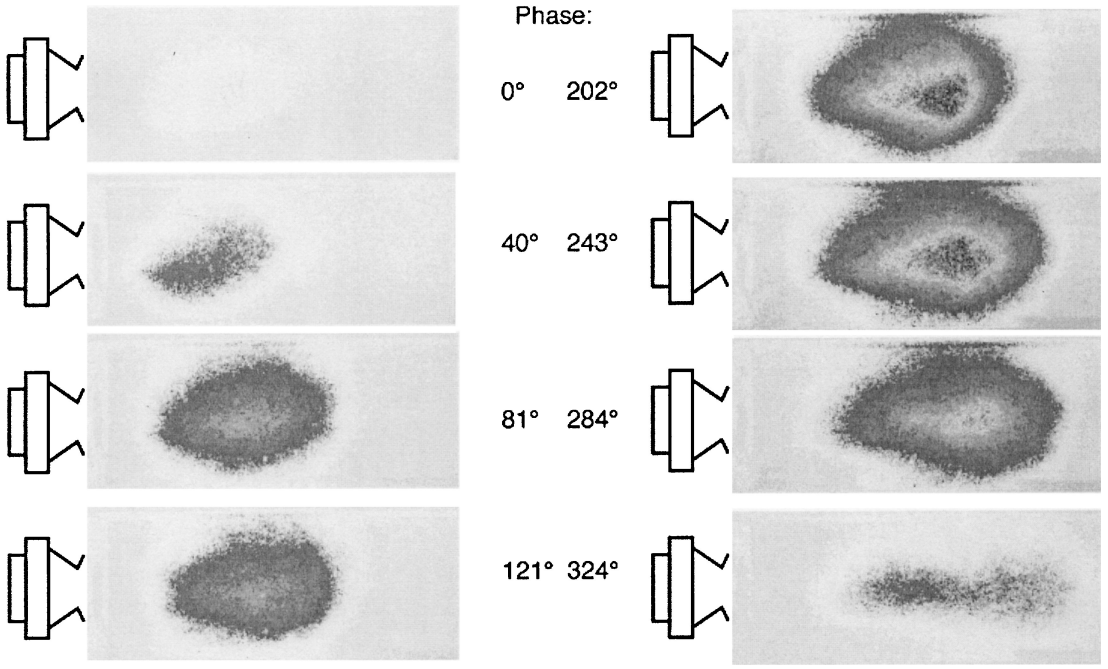

Fig. 11 Phase-locked images of CH* emission through the instability cycle, CNS. Regime J: CNS, P = 102 kW, Φ = 0.90, f = 350 Hz, and T_{inj} = 573 K.

and penetrates the injector element (Fig. 13). Heat is released in the near vicinity of the injector exhaust indicating that the flame now touches the injector. It is not possible to look inside this unit during operation, but there is some metal erosion so that the flame penetrates this element. This phenomenon corresponds to unsteady flashback and appears when the flame speed exceeds the flow velocity in the region located in the immediate vicinity of the injector. The regime only appears in the COS geometry for two reasons:

1) Instabilities in the COS configuration are established only for low injection velocities. This is favorable to an upstream propagation of the flame.

2) The COS geometry features a low-velocity region associated to the central recirculation core induced by the flow rotation. The axial velocity is quite low near the center line (see Ref. 20), where flashback occurs.

Flashback can also be linked to the convergent/divergent geometry of the injector. The phenomenon can be avoided with suitably shaped injectors operating in a stable mode. Flashback was apparently not observed by Snyder et al.,[28] who used a constant section injector with counterswirling blades, or by Döbbeling et al.,[29] who operated with a fully diverging injector, or by Puri et al.,[30] who worked with a converging-diverging nozzle. In the present experiments flashback prevails when the pressure oscillation has a large amplitude inducing flow deceleration and provoking the upstream propagation of the flame in regions where the velocity profile already features a local minimum. Although the difference in velocity distributions between the COS and CNS geometries is the most probable cause for their distinct behavior with respect to flashback, their can also be differences in fuel distributions that could contribute to this behavior.

Flashback conditions do not cause much damage to the injector mainly because the device is cooled by the continous flow of reactants. Some erosion takes place on the injector venturis. Operating with a 100-kW ceramic gas turbine combustor, Kumakura et al.[31] observed that flashback could lead to destruction of the flame holder. The difference in damage is related to injector design. In Ref. 31 the fuel–air mixture follows a curved flow before reaching the flame holder. The distance between fuel–air mixing and combustion zone is a critical parameter in flashback phenomenon.

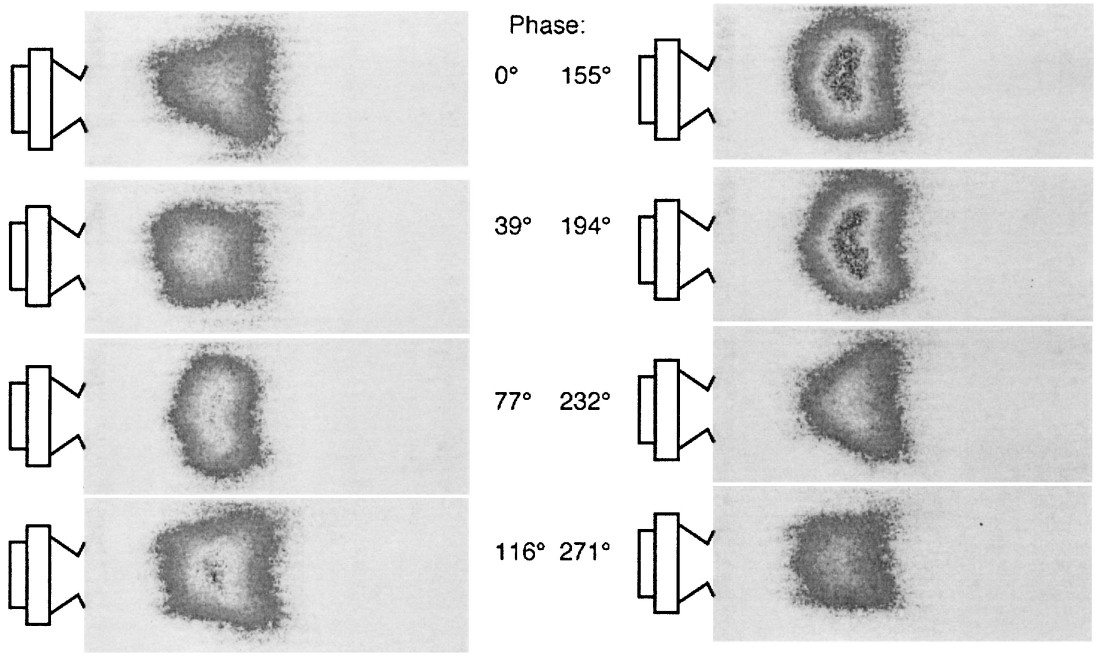

Fig. 12 Phase-locked images of CH* emission through the instability cycle. Regime K: COS, lifted flame, P = 69 kW, Φ = 0.94, T_{inj} = 573 K, and f = 430 Hz.

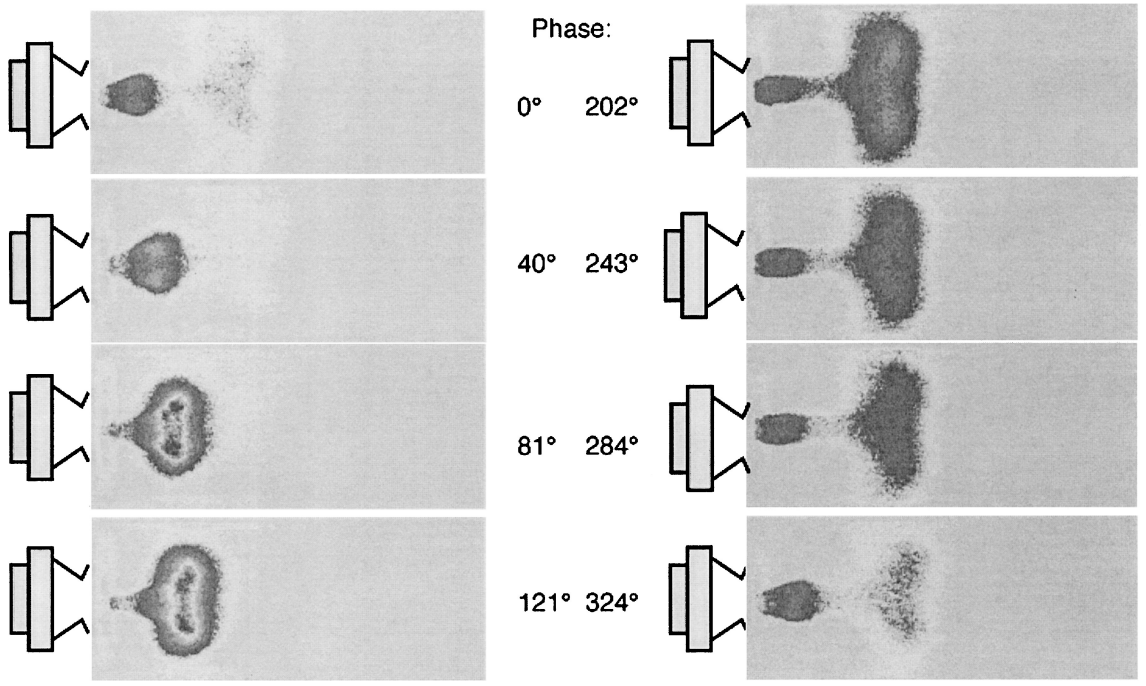

Fig. 13 Phase-locked images of CH* emission through the instability cycle. Regime L: COS, flashback, P = 33 kW, Φ = 0.52, T_{inj} = 523 K, and f = 450 Hz.

In the flashback regime, the reaction zone is close to the injection plane and near the flow axis, and the phase-resolved flame emission images are axisymmetric (Fig. 13). One can then compute the cross section of the reaction zone along the axis. The computerized tomography of the integrated heat release along the burner width is based on the Abel transform (for example, see Ref. 32) as applied in the recent work of Herding et al.[33] The result is displayed in Fig. 14. In the cross section thus obtained, a coherent vortical structure develops during the cycle. This vortex is generated near the axis. It is then expanding downstream (0- to 121-deg phase angle) while a new pattern appears in the LPP injector (phase 200 to 360 deg). When the vortex impinges on the duct walls (between 120 and 202 deg), breakdown takes place augmenting the level of fine grained turbulence, producing a pulse of heat and decelerating the incoming flow. The flame moves upstream. A new vortex is shed during the positive excursion of the flow velocity.

D. Mechanisms

Among the many possible mechanisms that can drive an instability in lean premixed combustors, one can distinguish two generic classes. In the first class, the flow develops large-scale structures like vortices that entrain a finite amount of fresh reactants and react at a later instant. A heat-release pulse is generated in the later stage when the vortex breaks down, impinges on a side wall, or interacts with another structure (for example, see Refs. 7 and 34). In the second class, the equivalence ratio is modulated by the pressure

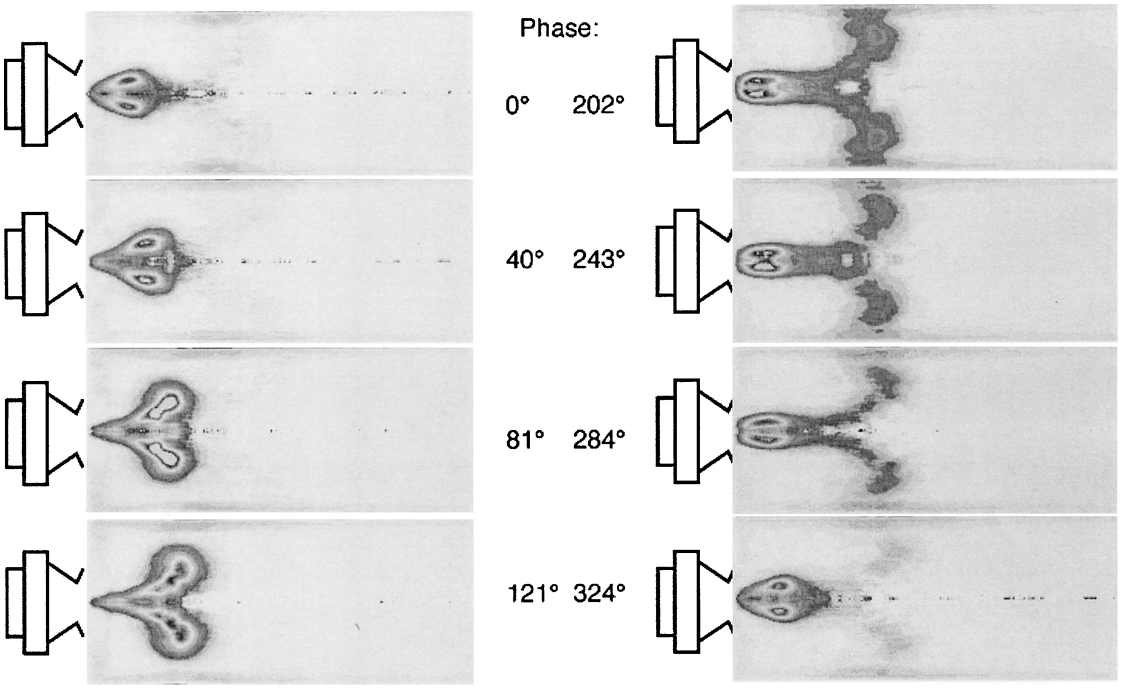

Fig. 14 Abel-deconvolution of the images shown in Fig. 13. Regime L. COS, flashback, P = 33 kW, Φ = 0.52, T_{inj} = 523 K, and f = 450 Hz.

oscillation existing in the combustor. The process involves the injector and is related to the difference in dynamical response of the fuel and air lines. The coupling between the combustor and its feed lines could be eliminated by increasing the head losses in the injection unit. Although this is possible in certain cases like rocket motors where the injector pressure drop is about 15% of the mean chamber pressure, such head losses are not acceptable in gas turbine applications. When the head loss is limited, coupling takes place, and the equivalence ratio is modulated by the pressure fluctuations existing in the sytem. The modulations are convected downstream, and heat is released at a later stage with a delay with respect to the fluctuation of equivalence ratio at the injector (for example, see Ref. 17).

Both mechanisms of instability involve a convective delay. In the first case, the delay is essentially related to the convection of the vortex structure inside the combustor $\tau_{\text{conv}} = l/u_{\text{conv}}$, where l is the characteristic distance of the flame region with respect to the inlet plane. This distance can be estimated from the average emission maps or more precisely from maps of Rayleigh index. Both methods provide similar values. These estimates remain somewhat arbitrary, but they are obtained here with the same method to allow comparisons. In the second case there is an additional delay as a result of convection inside the injector $\tau_{\text{conv}} = \tau_{\text{inj}} + l/u_{\text{conv}}$.

In addition to this convective delay, one has to account for a chemical time τ_c, which essentially depends on the fuel type, equivalence ratio Φ, and injection temperature T_{inj}. One can then define a total delay:

$$\tau_e = \tau_{\text{conv}} + \tau_c(\Phi, T_{\text{inj}}) \tag{2}$$

The delay associated with droplet vaporization is not included in this sum because evaporation takes place in parallel while the droplets are convected.

The convection velocity u_{conv} can be taken to be proportional to the inlet velocity $u_{\text{conv}} = \beta u$ with $\beta \sim 0.6$. The characteristic chemical time τ_c can be estimated from the early work of Zukoski.[35] It is found that $\tau_c \sim 0.15$ ms $\ll \tau_{\text{conv}} \sim 4$ to 7 ms. Using the estimated values of the total time lag τ_e, one can calculate the product $\tau_e f = \tau_e/T$. This quantity compares the delay to the instability period.

Table 1 gives estimates of the different time delays and the related characteristic ratios τ_e/T. In doing the calculations, it was assumed on the basis of the visualizations that COS instabilities were of the first type (vortex driven), whereas CNS instabilities were of the second type (equivalence-ratio inhomogeneity). In essence, this rough analysis indicates that the time delay involved in the instability process is of the order of a period of oscillation. It is found that τ_e/T is of order unity in both situations. It was suggested in Ref. 36 that instabilities are observed when the characteristic ratio τ_e/T was in a range of the form $[C_n - 1/4, C_n + 1/4]$, where C_n is a set of integers. This is true here for $(C_1 = 1)$ for both types of instabilities, those in which the process involves identifiable vortex patterns (COS) or those where there is no discernable flow structure but in which equivalence-ratio inhomogeneities probably prevail (CNS).

In developing the preceding estimates, our aim was only to propose a consistent framework for the observations made in the two swirl configurations. Because time-resolved measurements of the equivalence ratio are not easy to make in a mixture originating from a spray, they have not been attempted here, and it is not possible to confirm that CNS instabilities are related to equivalence-ratio inhomogeneities. It is indicated in Ref. 17 that instabilities driven by equivalence-ratio fluctuations are most effective for low values of the mean equivalence ratio and that their relative importance diminishes as this ratio is increased. This appears to be at variance with the present interpretation. One can note however that the mechanism mainly depends on the ratio of pressure fluctuation to the head loss inside the injection unit $p'/\Delta p_{\text{inj}}$. This ratio is of the order of one for the CNS instabilities, a value that is quite capable of inducing fluctuations in equivalence ratio.

IV. Conclusions

Combustion instabilities in a 150-kW premixed prevaporized burner fed with liquid fuel have been studied systematically. Two configurations are considered, based on co- and counterrotating internal swirl injectors. The following conclusions can be drawn concerning this particular system:

1) The frequencies of combustion instabilities are not strongly dependent on the injector configuration. They are mainly defined by the acoustic modes of the system but the exact value changes with the swirl geometry.

2) Instabilities move the reaction zone closer to the injector for about one-third of the stabilization distance in both co- and counterswirl configurations. This is because of a better mixing between fresh reactants and burnt gases, which accelerates the heat-release process.

3) The stable/unstable combustion domains differ for the two injector configurations. In the coswirl (COS) system, instabilities occur for velocities lower than a critical velocity, whereas they appear in the counterswirl (CNS) case for velocities in excess of a critical velocity. The critical velocity increases with Φ and T_{inj} in the COS geometry; it decreases with Φ and increases with T_{inj} in the CNS configuration.

4) Transition between stable and unstable regimes differ as well. In coswirl configuration where the reaction zone lies closer to the injector, the transition between stable and unstable regimes is quite sharp (within 4% of equivalence-ratio variation), whereas in counterswirl configuration it is less sensitive to airflow rate variation and appears more progressively with equivalence-ratio variation.

5) The overall instability process can be deduced from the phase-averaged images. In the coswirl configuration, the instability is generated by large vortical structures formed near the axis that break down at a later time producing a pulse of heat release. No structure is identified in the CNS configuration, but the reaction pattern propagates downstream, and the global reaction rate grows during this process. From this wave-like behavior and on the basis of a time-delay analysis, it is suspected that the instability is driven by equivalence-ratio inhomogeneities.

6) In the coswirl configuration and for low injection velocities and equivalence ratios, flashback was observed. This behavior is probably related to the presence of a region of minimum velocity near the flow axis close to the injector and induced by the higher swirl intensity in the coswirl geometry. When the pressure amplitude is high enough, the flow decelerates periodically, and the turbulent flame is able to propagate upstream along the flow axis and penetrate the injector.

Acknowledgments

Support for this research has been provided by the European community in the frame of the Brite Euram contract ACIACOC (BE97-4324). We wish to thank the anonymous reviewers for their many helpful comments.

References

[1]Correa, S. M., "A Review of NOx Formation Under Gas-Turbine Combustion Conditions," *Combustion Science and Technology*, Vol. 87, Nos. 1–6, 1992, pp. 329–362.

[2]Lefebvre, A. H., "The Role of Fuel Preparation in Low-Emission Combustion," *Journal of Engineering for Gas Turbine and Power*, Vol. 117, No. 4, 1995, pp. 617–654.

[3]Rayleigh, J. W. S., *The Theory of Sound*, Dover, New York, Vol. 2, 1945.

[4]Putnam, A. A., *Combustion-Driven Oscillations in Industry*, Elsevier, New York, 1971.

[5]Cowell, L. H., and Smith, K. O., "Development of a Liquid-Fueled, Lean-Premixed Gas Turbine Combustor," *Journal of Engineering for Gas Turbine and Power*, Vol. 115, No. 3, 1993, pp. 554–562.

[6]Candel, S., "Combustion Instabilities Coupled by Pressure Waves and Their Active Control," *Proceedings of the Combustion Institute*, Vol. 24, 1992, pp. 1277–1295.

[7]Schadow, K. C., and Gutmark, E., "Combustion Instability Related to Vortex Shedding in Dump Combustors and Their Passive Control," *Progress in Energy and Combustion Science*, Vol. 18, No. 2, 1992, pp. 117–132.

[8]Yang, V., and Anderson, W. E., *Liquid Rocket Engine Combustion Instability*, Vol. 169, AIAA, Washington, DC, 1995.

[9]Shih, W. P., Lee, J. G., and Santavicca, D. A., "Stability and Emissions Characteristics of a Lean Premixed Gas Turbine Combustor," *Proceedings of the Combustion Institute*, Vol. 26, 1996, pp. 2771–2778.

[10]Poinsot, T., Trouvé, A., Veynante, D., Candel, S., and Esposito, E., "Vortex-Driven Acoustically Coupled Combustion Instabilities," *Journal of Fluid Mechanics*, Vol. 177, 1987, pp. 265–292.

[11]Sivasegaram, S., and Whitelaw, J. H., "The Influence of Swirl on Oscillations in Ducted Premixed Flames," *Combustion and Flame*, Vol. 85, Nos. 1–2, 1991, pp. 195–205.

[12]Stephens, J., Acharya, S., and Gutmark, E. J., "An Experimental Study: Swirl-Stabilized Spray Combustion with Active Forcing," AIAA Paper 99-0330, Jan. 1999.

[13]Cha, M. S., Lee, D. S., and Chung, S. H., "Effect of Swirl on Lifted Flame Characteristics in Non Premixed Jets," *Combustion and Flame*, Vol. 117, No. 3, 1999, pp. 636–645.

[14]Yegian, D. T., and Cheng, R. K., "Development of a Lean Premixed Low-Swirl Burner for Low NOx Practical Applications," *Combustion Science and Technology*, Vol. 139, Nos. 1–6, 1998, pp. 207–227.

[15]Plee, S. L., and Mellor, A. M., "Review of Flashback Reported in Prevaporizing/Premixing Combustors," *Combustion and Flame*, Vol. 32, No. 2, 1978, pp. 193–203.

[16]Guin, C., "Characterization of Autoignition and Flashback in Premixed Injection Systems," *Proceedings of the 14th Symposium on Gas Turbine Combustion, Emissions and Alternative Fuels*, RTO, Neuilly, France, 1998.

[17]Lieuwen, T. C., Neumeier, Y., and Zinn, B. T., "The Role of Unmixedness and Chemical Kinetics in Driving Combustion Instabilities in Lean Premixed Combustors," *Combustion Science and Technology*, Vol. 135, Nos. 1–6, 1998, pp. 193–211.

[18]Dowling, A. P., "A Kinematic Model of a Ducted Flame," *Journal of Fluid Mechanics*, Vol. 394, 1999, pp. 51–72.

[19]Beer, J., and Chigier, N., *Combustion Aerodynamics*, Krieger, Malabar, FL, 1983.

[20]Bismes, F., and Trichet, P., "Detailed Spray Characterization," Brite Euram Low NOx III, TR, ONERA, France, 1998.

[21]Claypole, T. C., and Syred, N., "The Effect of Swirl Burner Aerodynamics on NOx Formation," *Proceedings of the Combustion Institute*, Vol. 18, 1980, pp. 81–89.

[22]Shu, Z., Krass, B. J., Choi, C. W., Aggarwal, S. K., Katta, V. R., and Puri, I. K., "An Experimental and Numerical Investigation of the Structure of Steady Two-Dimensional Partially Premixed Methane-Air Flames," *Proceedings of the Combustion Institute*, Vol. 27, 1998, pp. 625–632.

[23]Walsh, K. T., Long, M. B., Tanoff, M. A., and Smooke, M. D., "Experimental and Computational Study of CH, CH* and OH* in an Axisymmetric Laminar Diffusion Flame," *Proceedings of the Combustion Institute*, Vol. 27, 1998, pp. 615–623.

[24]LeHelley P., "Etude Théorique et Expérimentale des Instabilités de Combustion et de leur Contrôle dans un Brûleur Laminaire Prémélangé," Ph.D. Dissertation, Ecole Centrale Paris, France, June 1994.

[25]Poinsot, T., LeChatelier, C., Candel, S., and Esposito, E., "Experimental Determination of the Reflection Coefficient of a Premixed Flame in a Duct," *Journal of Sound and Vibration*, Vol. 107, No. 2, 1986, pp. 265–278.

[26]Venkataraman, K. K., Preston, L. H., Simons, D. W., Lee, B. J., Lee, J. G., and Santavicca, D. A., "Mechanism of Combustion Instability in a Lean Premixed Dump Combustor," *Journal of Propulsion and Power*, Vol. 15, No. 6, 1999, pp. 909–918.

[27]Richards, G. A., and Janus, M. C., "Characterization of Oscillations During Premix Gas Turbine Combustion," *Journal of Engineering for Gas Turbines and Power*, Vol. 120, No. 2, 1998, pp. 294–302.

[28]Snyder, T. S., Rosfjord, T. J., McVey, J. B., Hu, A. S., and Schlein, B. C., "Emission and Performance of a Lean-Premixed Gas Fuel Injection System for Aeroderivative Gas Turbine Engines," *Journal of Engineering for Gas Turbine and Power*, Vol. 118, No. 1, 1996, pp. 38–45.

[29]Döbbeling, K., Knöpfel, H. P., Polifke, W., Winkler, D., Steinbach, C., and Sattelmayer, T., "Low-NOx Premixed Combustion of MBtu Fuels Using the ABB Double Cone Burner (EV Burner)," *Journal of Engineering for Gas Turbine and Power*, Vol. 118, No. 1, 1996, pp. 46–53.

[30]Puri, R., Stansel, D. M., Smith, D. A., and Razdan, M. K., "Dry Ultralow NOx Green Thumb Combustor for Allison's 501-K Series Industrial Engines," *Journal of Engineering for Gas Turbine and Power*, Vol. 119, No. 1, 1997, pp. 93–101.

[31]Kumakura, H., Sasaki, M., Suzuki, D., and Ichikawa, H., "Development of a Low-Emission Combustor for a 100-kW Automotive Ceramic Gas Turbine (II)," *Journal of Engineering for Gas Turbine and Power*, Vol. 118, No. 1, 1996, pp. 167–172.

[32]Tatum, J. B., and Jaworski, W. A., "A Solution of Abel's Equation," *Journal of Quantitative Spectroscopy and Radiative Transfer*, Vol. 38, No. 4, 1987, pp. 319–322.

[33]Herding, G., Snyder, R., Rolon, C., and Candel, S., "Investigation of Cryogenic Propellant Flames Using Computerized Tomography of Emission Images," *Journal of Propulsion and Power*, Vol. 13, No. 2, 1998, pp. 146–151.

[34]Samaniego, J. M., Yip, B., Poinsot, T., and Candel, S., "Low-Frequency Combustion Instability Mechanisms in a Side-Dump Combustor," *Combustion and Flame*, Vol. 94, No. 4, 1993, pp. 363–380.

[35]Zukoski, E. E., "Afterburners," *Aerodynamics of Aircraft Engine Components*, edited by G. C. Oates, AIAA Education Series AIAA, New York, 1988, p. 76.

[36]Lieuwen, T., and Zinn, B. T., "The Role of Equivalence Ratio Oscillations in Driving Combustion Instabilities in Low NO_x Gas Turbines," *Proceedings of the Combustion Institute*, Vol. 27, No. 2, 1999, pp. 1809–1816.